A STUDY ON THE EFFECTS OF J_2 PERTURBATIONS ON A DRAG-FREE CONTROL SYSTEM FOR SPACECRAFT IN LOW EARTH ORBIT

Melissa Fleck Vess and Scott R. Starin
NASA Goddard Space Flight Center, Greenbelt, MD 20771

INTRODUCTION

Low Earth Orbit (LEO) missions provide a unique means of gathering information about many of Earth's aspects such as climate, atmosphere, and gravitational field. Among the greatest challenges of LEO missions are designing, predicting, and maintaining the spacecraft orbit. The predominant perturbative forces acting on a spacecraft in LEO are J_2 and higher order gravitational components, the effects of which are fairly easy to predict, and atmospheric drag, which causes the greatest uncertainty in predicting spacecraft ephemeris.[1] The continuously varying atmospheric drag requires increased spacecraft tracking in order to accurately predict spacecraft location. In addition, periodic propulsive maneuvers typically must be planned and performed to counteract the effects of drag on the spacecraft orbit. If the effects of drag could be continuously and autonomously counteracted, the uncertainty in ephemeris due to atmospheric drag would essentially be eliminated from the spacecraft dynamics.

One method of autonomous drag compensation that has been implemented on some missions is drag-free control. Drag-free control of a spacecraft was initially proposed in the 1960's and is discussed extensively by Lange.[2] His drag-free control architecture consists of a free-floating proof mass enclosed within a spacecraft, isolating it from external disturbance forces such as atmospheric drag and solar radiation pressure. Under ideal conditions, internal disturbance forces can be ignored or mitigated, and the orbit of the proof mass depends only on gravitational forces. A sensor associated with the proof mass senses the movement of the spacecraft relative to the proof mass. Using the sensor measurements, the spacecraft is forced to follow the orbit of the proof mass by using low thrust propulsion, thus counteracting any non-gravitational disturbance forces. If the non-gravitational disturbance forces are successfully removed, the spacecraft's orbit will be affected only by well-known gravitational forces and will thus be easier to predict.

With the elimination of drag, the dominant perturbations acting on a LEO spacecraft are higher order gravitational components. The Earth has a bulge at the equator, is slightly pear shaped, and has a slight flattening of the poles.[3] This asphericity, in addition to asymmetric density, contributes to a non-uniform geopotential function, the gradient of which yields the total gravitational acceleration of the spacecraft. In LEO, the dominant gravitational perturbation term is J_2, which represents the oblateness of the Earth. The J_2 gravitational term is almost 1000 times larger than the next largest term, J_3.[4]

The authors have previously written a paper dealing with drag-free control in the context of single LEO spacecraft.[5] That first paper represented part of a study to determine the feasibility of a generic, low-cost drag-free control system for spacecraft in LEO. The current work presents new results from that ongoing study. The first paper compared the total orbital velocity changes (ΔV) required for two orbital maintenance regimes: drag-free control and periodic orbit boosts at up to 4-week intervals. That comparison demonstrated that drag-free control could yield significant fuel savings for high-drag missions (*i.e.* low altitude, low ballistic coefficient). The paper also presented trends of drag-free effectiveness based on mission characteristics (*e.g.* altitude, inclination) that could be used by engineers to make judgments in the context of their own professional interest, be that research and development or space mission design. The study made use of a spherical-Earth assumption, so that there were no J_2 perturbations, to establish clear relationships between the spacecraft orbital characteristics and concomitant drag effects, and the usefulness of drag-free control.

The current paper explores the effects of J_2 perturbations on drag-free control of a spacecraft in LEO. As in the first paper, a simulated drag-free control system is used to establish comparisons and trends between various LEO, drag-free scenarios. Because J_2 is a gravitational perturbation and affects both the spacecraft and proof mass, the only

difference between the spacecraft and proof mass equations of motion is drag acceleration acting on the spacecraft. The drag-free control system should be able to remove the effects of that drag acceleration, leaving only Keplerian motion perturbed by the effects of J_2. In particular, this paper attempts to explain any extra ΔV costs associated with the inclusion of J_2 perturbations in the drag-free control simulation.

SIMULATION

The drag-free controller and test simulation were created using Simulink, and can be separated into four main parts: spacecraft orbit, proof mass orbit, gap measurement, and the drag-free controller.

Spacecraft Orbit

The spacecraft in this simulation is assumed to be nadir-pointing and in a low-eccentricity, low-Earth orbit with inclination varied between cases. Initial orbit parameters were calculated for a circular Keplerian orbit, as was done in [5]. However, as a result of the presence of an increased and asymmetric potential due to J_2 this initialization procedure resulted in non-circular orbits. Once initialized, the spacecraft orbit is propagated in the inertial frame using two-body orbit dynamics with atmospheric drag and J_2 perturbations.

The atmospheric density values used are the average density values listed in [3], with linear interpolation between data points. Solar radiation pressure is not included because below altitudes of 800 km atmospheric drag is dominant;[3] this study considers altitudes only up to 700 km. The total spacecraft acceleration is the sum of the two-body, drag, J_2, and commanded acceleration vectors and is integrated using a fixed-step, fifth-order Runge-Kutta solver to obtain the velocity and position of the spacecraft. Initial position and velocity vectors are calculated from simulation-specific initial conditions. The integration step size is 10 seconds. The new spacecraft position and velocity vectors are then used to calculate the new two-body, drag, and J_2 accelerations. The commanded acceleration comes from the drag-free controller.

Proof Mass Orbit

In the drag-free control system modeled here, the proof mass is assumed to be a point mass and enclosed within a small, cubic cage or box. However the proof mass itself is not constrained along any axis; the proof mass is allowed to float freely within its enclosure. Because the proof mass is enclosed within the spacecraft, atmospheric drag does not affect the proof mass orbit. The proof mass orbit, therefore, is modeled using only gravitational accelerations, namely, two-body orbit dynamics with J_2 perturbations. The total proof mass acceleration is integrated to yield the proof mass position and velocity vectors. As with the spacecraft, initial position and velocity vectors are calculated from simulation-specific initial conditions.

Gap Measurement

It is assumed that there exists a sensor (*e.g.* capacitive or optical) that can measure the gap between the proof mass and the sides of its enclosure. That gap vector is a representation of how far apart the spacecraft and proof mass centers of mass are.[†] If the proof mass is located at the spacecraft center of mass and the proof mass and spacecraft are following exactly the same orbit, the proof mass will be located at the exact center of the box and the gap vector will be the target gap vector, which, in this system, is assumed to be $[1.0\ 1.0\ 1.0]^T$ cm – the center of a 2.0 cm cube.

The gap vector is measured in the spacecraft body frame. Because the spacecraft is assumed to be nadir pointing, the spacecraft body frame will also be the orbit frame. The gap vector is calculated by first subtracting the proof mass position vector from the spacecraft position vector, in the inertial frame. The position vector difference is then converted to the orbit (body) frame. The position vector difference in the orbit (body) frame must then be converted to a gap measurement:

[†] Note that, though there is in this paper no practical distinction made between a "center of mass" and a "center of gravity," the development of real drag-free sensors and the consideration of certain other perturbative effects would require proper attention to any difference between these locations in the spacecraft.

$$gap_m = gap_t - (r^o_{S\_P} + r_{P0}) \quad (1)$$

where gap_m is the measured gap vector, gap_t is the target gap vector of $[1.0\ 1.0\ 1.0]^T$ cm, $r^o_{S\_P}$ is the proof mass to spacecraft vector in the orbit frame, and r_{P0} is the offset of the proof mass cage from the spacecraft center of mass.

Each axis of the vector calculated above is limited to between 0.0 and 2.0 cm because the proof mass is enclosed within a 2.0 cm cube. If the gap were outside of those limits, the proof mass would be outside of the cube. At this point in the proof of concept study, drag-free sensor biases due to mass attraction between the proof mass and spacecraft are not included. As the study progresses, those biases will be introduced along with other error sources.

Drag-Free Controller

The acceleration needed to keep the spacecraft following the proof mass orbit is calculated with the drag-free controller using the gap vector components as inputs. A continuous, Proportional-Integral-Derivative (PID) controller is used on the three uncoupled axes of control, and the thrust vector is calculated from the vector sum of the three PID outputs. The PID gain matrices have not been optimized at this point in the study, but they have been selected to prevent the proof mass from ever hitting the side of the proof mass cage. The gains also do not consider optimizing the total thrust direction to minimize the ΔV applied.

SIMULATION SCENARIOS

To test the effectiveness of the drag-free controller and the effects of J_2 on drag-free controllability, two different scenarios were established. All cases in the scenarios were run for a four-week period. A summary of the two scenarios is shown in Table 1. In both scenarios, the attitude of the spacecraft is assumed to be nadir pointing and perfectly controlled.

Table 1: Summary of initial spacecraft parameters for Scenarios 1 & 2.

Initial Spacecraft Parameters				
	Scenario 1		Scenario 2	
Altitude	Varies	350 - 700 km	Varies	350 - 700 km
Inclination	Varies	0 - 60 deg	Varies	0 - 60 deg
Ballistic Coeff.	Varies	25 - 200 kg/m^2	N/A	
Eccentricity	Fixed	0	Fixed	0
RAAN	Fixed	0 deg	Fixed	0 deg
Arg. of Perigee	Fixed	0 deg	Fixed	0 deg
True Anomaly	Fixed	0 deg	Fixed	0 deg
J2 Perturbations	Yes		Yes	

Scenario 1

Scenario 1 assumes that the center of the proof mass cube is located at the center of mass of the spacecraft and that J_2 gravitational perturbations are acting on the spacecraft and proof mass. In addition, atmospheric drag is perturbing the spacecraft orbit. The goal of this scenario is to determine the effectiveness of the drag-free control concept with the addition of J_2 perturbations. Since J_2 is a gravitational acceleration, it will affect both the spacecraft and the proof mass orbits. The only simulated difference between the spacecraft and proof mass orbits is the atmospheric drag acceleration acting on the spacecraft, which is the effect the drag-free controller is attempting to remove. A total of 448 different cases were run for this scenario.

Scenario 2

Scenario 2 also assumes that the center of the proof mass cage is located at the center of mass of the spacecraft and that J_2 gravitational perturbations are acting on the spacecraft and proof mass. Atmospheric drag, however, is *not* acting on the spacecraft. This scenario is equivalent to perfect drag compensation with J_2 still present. It serves as a point of comparison for Scenario 1. Ideally, if drag is successfully removed, the orbits in Scenario 1 should closely match those of Scenario 2. A total of 56 cases were run for this scenario. Because J_2 perturbations do not depend on C_B, that parameter was not varied.

SIMULATION RESULTS

Each case within the two scenarios was run for a total of four weeks of simulated time. At the end of each simulation, the last 24 hours of position and velocity data at each integration time step were saved in files. Using the last 24 hours of a four-week simulation ensures that the controller has settled and the spacecraft orbit has reached its steady state. Between the two scenarios, a total of 504 different cases were tested. Due to this large amount of information, it is difficult to discuss all of the results in detail. This section, therefore, summarizes the main trends in the scenario results and the discoveries to which those trends lead.

Comparison of ΔV Cost of Drag-Free Control: J_2 vs. No J_2

In the earlier paper, the theoretical fuel cost of drag-free control is established in terms of cumulative ΔV obtained by integrating the acceleration from the drag-free controller.[5] This ΔV cost assumes no perturbations in the system other than drag acceleration acting on the spacecraft, which flies in a Keplerian orbit. This paper makes some comparisons between the ΔV costs of drag-free control for J_2 spacecraft and Keplerian spacecraft (no J_2; presented in [5]). Table 2 presents a sampling of these ΔV costs. Notice that in all cases, the ΔV cost for the J_2 spacecraft is larger than for the Keplerian spacecraft; this trend results mainly from the J_2 potential causing the J_2 spacecraft to dip lower in the atmosphere, which increases drag. This effect is discussed more thoroughly below.

Table 2: Comparison of ΔV totals from drag-free control simulations with and without J2 perturbations.

Comparison of ΔV Totals for a SC with C_B = 50 kg/m^2: J_2 (Scenario 1) vs. Keplerian (Fleck & Starin)						
	Inc = 0 deg		Inc = 30 deg		Inc = 60 deg	
Initial Altitude	ΔV With J2	ΔV Without J2	ΔV With J2	ΔV Without J2	ΔV With J2	ΔV Without J2
(km)	(m/s)	(m/s)	(m/s)	(m/s)	(m/s)	(m/s)
350	13.569	10.004	13.117	10.004	12.213	10.004
400	5.066	3.870	4.914	3.870	4.611	3.870
450	2.036	1.596	1.980	1.596	1.869	1.596
500	0.861	0.686	0.839	0.686	0.794	0.686
550	0.380	0.308	0.371	0.308	0.352	0.308
600	0.175	0.144	0.171	0.144	0.163	0.144
650	0.084	0.071	0.083	0.071	0.079	0.071
700	0.043	0.037	0.043	0.037	0.041	0.037

Equatorial Orbits

The relatively large increase in ΔV cost for the J_2 spacecraft did not intuitively make sense for the spacecraft in the equatorial orbit. J_2 is a zonal harmonic and as such is symmetric about the polar axis and dependent only on latitude.[4] A spacecraft in a circular equatorial orbit will not cross any latitude lines, and therefore it should see a

constant magnitude acceleration, assuming drag is compensated for and therefore the spacecraft altitude remains constant. Intuitively then, the ΔV cost for a J_2 spacecraft in a circular, equatorial orbit might be thought the same as the ΔV cost for the same spacecraft, at the same altitude, in a Keplerian orbit. It can be shown, however, that the difference in ΔV cost for the two circular, equatorial spacecraft orbits (Keplerian *vs.* J_2) will not be the same, nor will it be as large as what is seen in Table 2.

Consider the method in which the spacecraft initial position and velocity vectors are calculated. Originally, the spacecraft and proof mass initial conditions were defined in terms of apogee and perigee altitude, inclination, right ascension of the ascending node, argument of perigee, and true anomaly. Apogee and perigee were defined to be the same (equal to the spacecraft altitude), making the orbit circular. Initial position and velocity were then calculated by converting the classical orbital elements into Cartesian elements, (*i.e.* inertial position and velocity vectors) using methods derived from Kepler's laws. The resulting velocity, the Keplerian velocity, is the velocity required to maintain a circular Keplerian orbit of a given radius. This circular orbit may be maintained at any inclination about a spherical and uniform central body. However, when J_2 perturbations are present, the central body is neither spherical nor of uniform density. The geopotential function is non-uniform and the spacecraft orbit is therefore called non-Keplerian. With J_2 perturbations present, the geopotential is greater about the equator than in the spherical case, and the Keplerian velocity is not enough to maintain a circular orbit of a given altitude at the equator. The orbit of the spacecraft in Table 2, therefore, is not in a circular orbit at a constant altitude.

To calculate the velocity needed to maintain that circular orbit, the J_2 potential must be used to find the centripetal, gravitational acceleration. First we calculate the unit vector, $\hat{V}$, associated with the Keplerian velocity vector. Then calculate the Keplerian acceleration, $\boldsymbol{a}_K$, of the spacecraft or proof mass:

$$\boldsymbol{a}_K = -\frac{\mu}{r^3}\boldsymbol{r}, \tag{2}$$

where μ is the Earth's gravitational constant, $\boldsymbol{r}$ is the spacecraft or proof mass position vector in the inertial frame, and r is the magnitude of $\boldsymbol{r}$. The additional acceleration caused by J_2, $\boldsymbol{a}_{J2}$, can then be calculated:

$$\boldsymbol{a}_{J2} = -\frac{3J_2\mu R_E}{2r^5}\left(1-\frac{5r_z^2}{r^2}\right)\left(r_x\hat{i}+r_y\hat{j}\right)-\frac{3J_2\mu R_E}{2r^5}\left(3-\frac{5r_z^2}{r^2}\right)r_z\hat{k}, \tag{3}$$

where J_2 is the zonal coefficient due to the Earth's oblateness, R_E is the average radius of the Earth, and r_x, r_y, and r_z are the components of the spacecraft or proof mass position vector in the inertial frame, with principle directions $\hat{i}$, $\hat{j}$, and $\hat{k}$.[4] Because the magnitude of $\boldsymbol{a}_{J2}$ is constant at the equator, the two acceleration vectors can then be summed to determine the total acceleration acting on the spacecraft or proof mass at any point in the orbit. The total velocity magnitude, V_{J2}, needed to maintain a circular orbit of size r about the equator with J_2 perturbations present is then:

$$V_{J2} = \sqrt{a_T \cdot r}, \tag{4}$$

where a_T is the magnitude of the total acceleration acting on the spacecraft or proof mass. The initial spacecraft or proof mass velocity vector is then obtained by multiplying V_{J2} by the unit vector, $\hat{V}$. The resulting velocity vector, along with the position vector used in the above calculations, are the initial conditions that will be propagated in the simulation. Calculating the initial position and velocity vectors for the spacecraft and proof mass in this manner will ensure that the drag-free controller can maintain a circular orbit of a given altitude about the equator in the presence of J_2 perturbations.

It is important to note that the velocity magnitude calculated above will be *larger* than the velocity needed to maintain a Keplerian orbit. Recall that the equation for drag acceleration is:

$$\boldsymbol{a}_D = -\frac{1}{2C_B}\rho V^2 \hat{\boldsymbol{V}}, \tag{5}$$

where $\boldsymbol{a}_D$ is the acceleration due to drag, ρ is the atmospheric density, and C_B is the ballistic coefficient, which is equal to the mass of the spacecraft divided by its drag area. Atmospheric density is dependent on a spacecraft's position above the Earth, or the magnitude of the instantaneous position vector. By calculating the initial conditions using the above method, the position vector and therefore atmospheric density will be the same for the Keplerian and circular-J_2 spacecraft. However, as was mentioned before, the velocity of the circular-J_2 spacecraft will actually be greater, resulting in a larger atmospheric drag and thus a greater ΔV cost. The ΔV needed by a drag-free circular-J_2 spacecraft, ΔV_{J2}, can be estimated given the ΔV cost of a drag-free Keplerian spacecraft, ΔV_K, and the Keplerian and circular J_2 velocities, V_K and V_{J2}, respectively:

$$\Delta V_{J2} = \frac{V_{J2}^{\ 2}}{V_K^{\ 2}} \cdot \Delta V_K \,. \tag{6}$$

The ΔV cost is found with a simple ratio because the Keplerian and circular-J_2 spacecraft will be at the same altitude and thus have the same atmospheric density. Table 3 shows the predicted ΔV cost of a circular-J_2 spacecraft compared to that of a Keplerian spacecraft and the Scenario 1-J_2 spacecraft. Figure 1 shows the position magnitude, velocity magnitude, and drag acceleration magnitude *vs.* time for a Keplerian and circular-J_2 spacecraft in a 350 km, equatorial orbit and the Scenario 1-J_2 spacecraft. As can be seen in Figure 1, the Scenario 1-J_2 spacecraft does not maintain a circular orbit; it dips further into the atmosphere than does the Keplerian or circular-J_2 spacecraft. Furthermore, its velocity also oscillates, becoming larger than that of the Keplerian or circular-J_2 spacecraft. This oscillation in the instantaneous position and velocity magnitudes explains the larger increase in ΔV cost for the Scenario 1-J_2 spacecraft.

Table 3: Comparison of predicted ΔV totals for drag-free circular-J_2 spacecraft to ΔV totals for drag-free Keplerian and Scenario 1- J_2 spacecraft.

Comparison of ΔV Totals: J2 *vs.* Keplerian Inc = 0 deg, C_B = 50 kg/m²			
Altitude	**J2 ΔV (Scenario 1)**	**Keplerian ΔV (Fleck & Starin)**	**Predicted J2 ΔV (circular)**
(km)	(m/s)	(m/s)	(m/s)
350	13.569	10.004	10.019
400	5.066	3.870	3.875
450	2.036	1.596	1.598
500	0.861	0.686	0.687
550	0.380	0.3076	0.3080
600	0.175	0.1437	0.1439
650	0.084	0.0707	0.0708
700	0.043	0.03706	0.03711

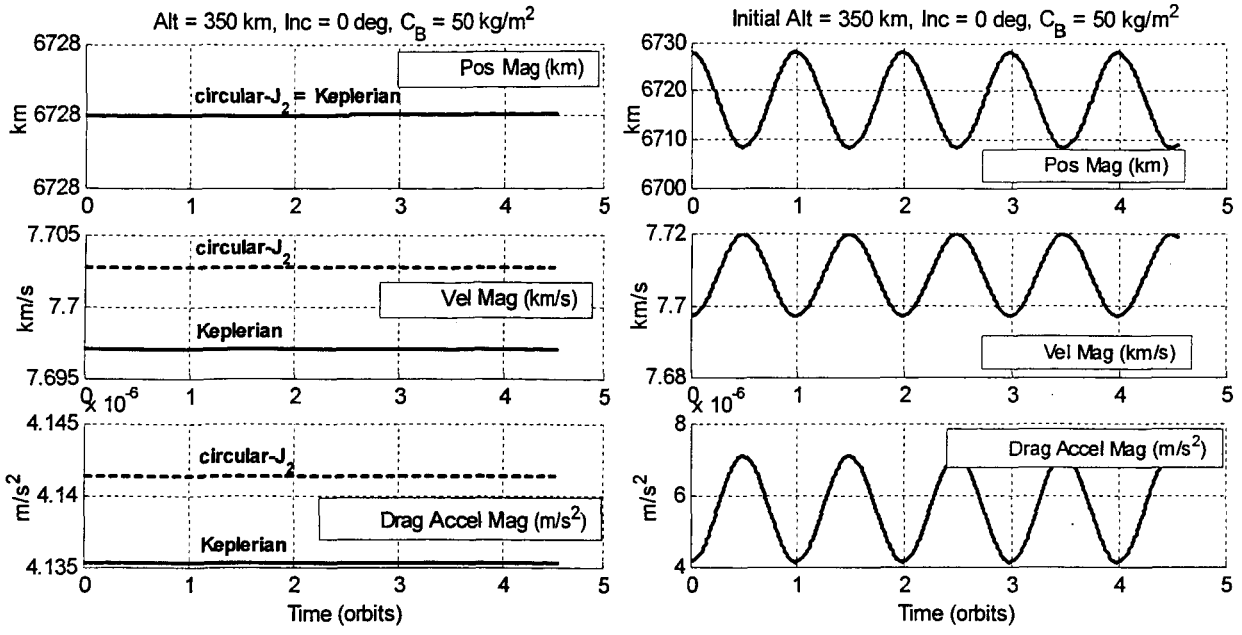

Figure 1: Position magnitude, velocity magnitude, and drag acceleration magnitude vs. time for a 50 kg/m^2 spacecraft with initial altitude of 350 km at. Left plot shows the circular-J_2 and Keplerian spacecraft. Right plot shows the Scenario 1-J_2 spacecraft.

Inclined Orbits

The analysis above shows that it is possible to maintain a circular orbit in the presence of J_2 perturbations for an equatorial orbit. The ΔV cost from that circular-J_2 case can then be compared to the ΔV cost of the Keplerian case. If the spacecraft orbit is inclined, however, it is not possible to maintain a circular orbit in the presence of J_2 perturbations. An inclined orbit will cross over different latitude lines, which will cause variation in the magnitude of the J_2 acceleration. This variation in the J2 acceleration will cause the position and velocity of the spacecraft to oscillate about some mean value. Given the exponential decay in atmospheric density (and thus atmospheric drag) with spacecraft altitude, the ΔV cost of the J_2 spacecraft should be greater than the ΔV cost of its Keplerian counterpart. This increase in ΔV cost is, in fact, the trend that is seen in Table 2.

Comparison of ΔV Cost of Drag-Free Control at Varying Inclinations

Also of interest from the results of Scenario 1 is the variation in ΔV cost as the orbital inclination increases for a given initial altitude. However, because of the inconsistency in orbital perturbations from one inclination to the next—the very inconsistency which would produce interesting comparisons—it is not clear what orbits should be compared. For example, an equatorial orbit may still be circular without any spacecraft guidance required; however, any nonzero inclination results in a non-circular orbit that defies accurate description in terms of Keplerian coordinates. So, starting both the equatorial and inclined orbits at the same altitude for purposes of comparison, as done in this study, produces orbits that experience very different density and velocity profiles over the course of even a single orbit. The drag is proportional to both atmospheric density (strongly influenced by altitude) and the square of orbital velocity, and yet both of these vary in every natural, inclined, J_2-influenced orbit. Evaluations of drag-free performance at various orbital inclinations were included in [5]. These evaluations led to a conclusion that inclination was not a strong influence on drag-free performance in Keplerian orbits. From the results presented here, it is clear that inclination plays a more important role when J_2 perturbations are present. Because of the spherical asymmetry, direct comparisons of an inclined orbit with and without J_2 are difficult, and potentially misleading. This does not diminish the value of the J_2 spacecraft results on their own; for instance, it is possible to make

comparisons to find trends due to altitude or other orbital characteristics within the subset of simulated cases at each particular inclination.

With this knowledge, it becomes clear that any comparison between the results from Scenario 2 and the previous work in [5] must be made carefully. As can be seen in Figures 1 and 2, the initial conditions calculated for each case in Scenario 1 ensure that the *maximum* altitude, and not the *mean* altitude, of the Scenario 1-J_2 spacecraft is the same as the Keplerian spacecraft. A comparison might be made between the ΔV cost of a Keplerian spacecraft at a given inclination and altitude and the ΔV cost of a J_2 spacecraft at the same inclination, whose *mean* altitude is the same as that of the Keplerian spacecraft. That is, the instantaneous orbits of the two spacecraft would be different, but their mean orbit would be the same. Whether this constitutes an appropriate comparison for any particular mission would depend on the answers to mission-specific questions: *e.g.* the accuracy of initial orbital placement by the launch vehicle, tolerance of the spacecraft to altitude variations.

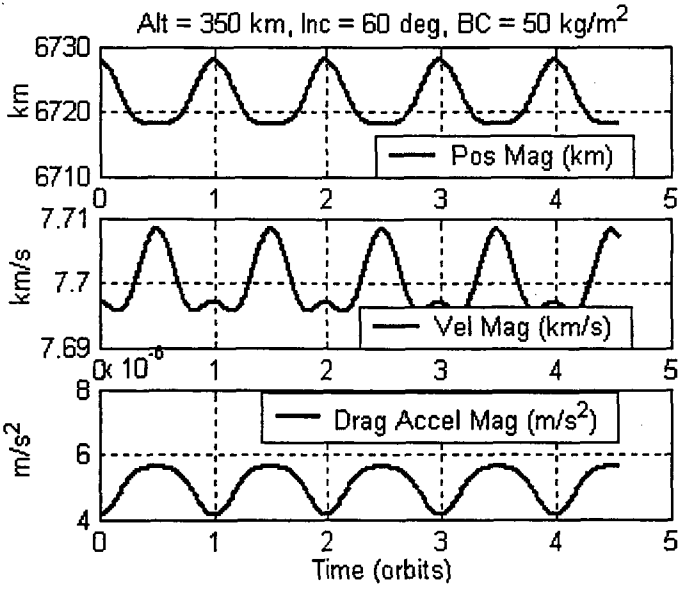

Figure 2: Position, velocity, and drag acceleration magnitude of a 50 kg/m2 Scenario 1-J_2 spacecraft with initial (maximum) altitude of 350 km and initial inclination of 60°.

Effectiveness of the Drag-Free Controller

To determine the effectiveness of the drag-free controller at removing drag with J2 perturbations present, the last 24 hours worth of position and velocity vectors from Scenarios 1 and 2 were saved for comparison. Because it was established that Cartesian elements cannot be converted to classical orbital elements with J2 present, all comparisons were made directly with the position and velocity vectors. Since Scenario 2 has no drag acceleration acting on the spacecraft, it was used as the baseline. At any instant in time, the position vector of the Scenario 2 (no drag) spacecraft represents where the Scenario 1 (drag) spacecraft is supposed to be. The velocity vector of the no drag spacecraft represents how fast and in what direction the drag spacecraft is supposed to be moving. Cases in Scenario 1 were compared to the corresponding cases in Scenario 2 to determine how well the controller is working to keep the drag spacecraft where it is supposed to be and moving as fast as it is supposed to be.

In determining controller effectiveness, the first thing that was done was to determine the overall worst-case errors in position and velocity. These errors are made up of two separate parts: error in magnitude and error in direction. The position and velocity magnitude errors were determined by subtracting the drag spacecraft position or velocity vector from that of the no drag spacecraft and taking the magnitude of that error vector. The position and velocity direction errors were determined by finding the angle between the drag and no drag position or velocity vector. For

Table 4: Overall worst-case errors between the position and velocity vectors: Scenario 1 *vs.* Scenario 2

Overall Worst-Case Errors from Drag-Free Control Simulation with J_2 Perturbations				
	Error	Initial Altitude	Initial Inclination	Ballistic Coefficient
		(km)	(deg)	(kg/m^2)
Position Magnitude (mm)	6.359E-02	350	30	25
Position Angle (arcsec)	6.873E-03	350	20	125
Velocity Magnitude (mm/s)	8.910E-05	350	0	25
Velocity Angle (arcsec)	7.529E-03	700	10	50

a given case, the magnitude and direction of the errors were determined at each 10-second time step. The worst-case errors *for that case* would then be the maximum position and velocity errors. The *overall* worst-case errors would then be the maximum position and velocity errors of all the cases studied. Those errors and the case from which they come are shown in Table 4. As can be seen, over a four-week time span the drag-free controller does a good job of removing drag from the spacecraft. All of the overall maximum errors except velocity angle occur at the lowest initial altitude tested, 350 km. The maximum errors occur for an initial altitude of 350 km, since drag acceleration is greater at lower altitudes.

Of interest also are the instantaneous errors in position and velocity within any given case. Given the number of cases run, it would be impossible to discuss these errors in detail for every case. Therefore, this discussion will focus on the general trends seen in the cases studied. Figure 3 shows a representative example of the position and velocity errors. These particular errors are for a 100 kg/m^2 spacecraft at an initial altitude of 450 km and an initial inclination of 30° for the last 12 hours of the 4-week simulation; the 12 hour period is chosen for clarity of the figure. As can be seen in the figure, the position and velocity magnitude errors oscillate fairly regularly with the orbit of the spacecraft. This stable oscillation implies that the controller has reached a steady state limit cycle, and the errors should not grow any larger. The errors in position and velocity angle appear to be related to numerical simulation of the 10-second thrust interval, and they are bounded and extremely small. Again, the fact that these

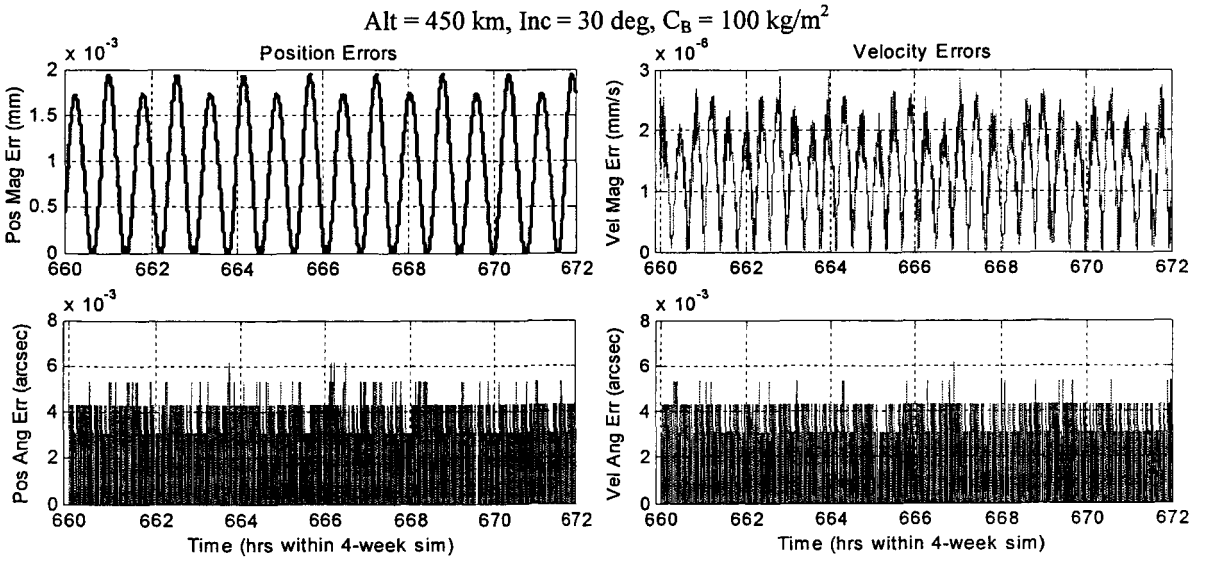

Figure 3: Position and velocity errors for the last 12 hours of the 4-week simulation.

errors are bounded over the last 12 hours of the simulation implies that these errors will not grow as additional time goes by. It is important to reiterate that the simulation does not include any noise at this point. The fact that the errors are bounded does not imply that the controller is robustly stable. It simply shows, as is the goal of this study, that the concept of drag-free control is possible from an ideal standpoint.

Another thing that is interesting to point out in discussing the effectiveness of the drag-free controller is how the magnitude errors vary within the orbit of the spacecraft. Figure 4 shows the position magnitude error plotted *vs.* the X- and Y-components of the no drag spacecraft position vector for the last 24 hours of the case with an initial altitude of 450 km, initial inclination of 0°, and spacecraft C_B of 100 kg/m^2. In addition, the bold line shows the orbit of the no drag spacecraft, *i.e.* the ideal orbit. The position magnitude error can be shown in this fashion because the orbit is un-inclined, and there is no Z-component of the position vector. As can be seen in the figure, for each orbit the position magnitude error reaches a peak four times and drops to approximately zero between those peaks. The oscillation in the position magnitude error repeats with each orbit, showing again the controller limit cycle discussed earlier.

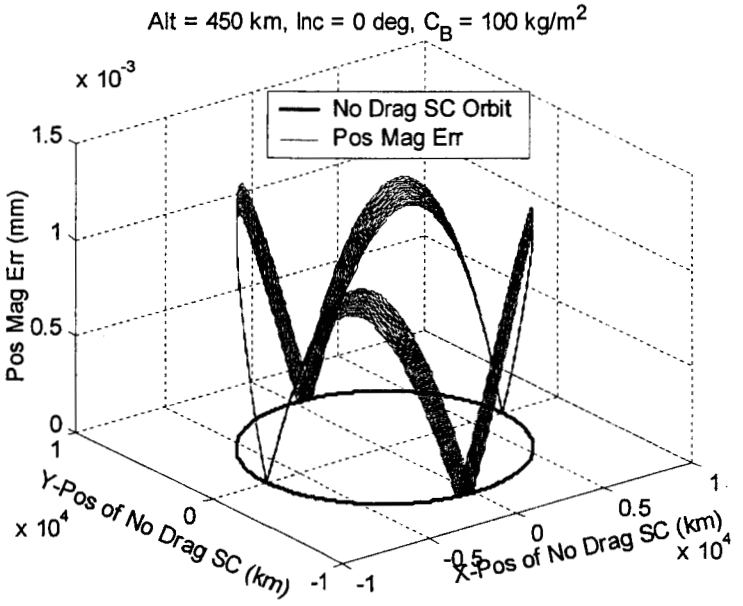

Figure 4: Plot of the position magnitude error as a function of the location along the no drag spacecraft orbit. The bold circle shows the orbit of the no drag spacecraft.

CONCLUSION

A Simulink simulation was developed to look at the effects of J_2 perturbations on a drag-free control system for spacecraft in LEO. Two different scenarios were developed to test the simulation. Scenario 1 assumes that drag and J_2 perturbations are acting on the spacecraft, whereas Scenario 2 assumes only J_2 perturbations acting on the spacecraft, representing "perfect" drag compensation. A comparison of the results from Scenarios 1 and 2, along with results from an earlier study by the authors, led to the following conclusions.

A comparison of Scenarios 1 and 2 shows that the drag-free controller can remove drag from the spacecraft orbit with J_2 perturbations present. After four weeks, overall worst-case errors in position and velocity magnitude are 0.06 mm and 9.0e-5 mm/s, respectively. In addition, worst-case errors in position and velocity direction are on the order of thousandths of an arc second. The instantaneous errors in position and velocity magnitude show that the errors are bounded and oscillate with respect to the spacecraft orbit.

The ΔV cost of maintaining a circular, equatorial orbit, with drag-free control, in the presence of J_2 perturbations will be slightly higher than maintaining the same orbit without J_2 perturbations. The added ΔV cost comes from the fact that additional velocity is required to maintain a circular, equatorial orbit with J_2 present. As drag acceleration is dependent on velocity squared, that additional velocity translates to additional drag, and therefore additional ΔV to counteract that drag.

To compare the ΔV cost of drag-free control for J_2-spacecraft to that of Keplerian spacecraft in inclined orbits, care must be taken to ensure that the *mean* J_2-spacecraft altitude is the same as the altitude of the Keplerian spacecraft. In that case, the ΔV cost of J2-spacecraft will also be greater than the ΔV cost of the Keplerian spacecraft. This increase in ΔV cost is because the J_2 spacecraft position will oscillate about the mean altitude, and atmospheric density (and thus atmospheric drag) decreases *exponentially* with instantaneous spacecraft altitude. Therefore, time spent *below* the mean altitude will provide a greater contribution to the ΔV cost than will time spent *above* the mean altitude, resulting in an overall greater ΔV cost than the Keplerian spacecraft.

The authors were originally interested in comparing drag-free controller performance and ΔV cost across different orbital inclinations. However, because J_2 perturbations vary across geocentric latitude, spacecraft at different inclinations will experience vastly different position (therefore density) and velocity profiles. These different orbits make it difficult to draw generalized conclusions about the effects of varying inclination on the controller performance and ΔV cost. If, however, the spacecraft orbit were established such that the mean spacecraft altitude were the same across all inclinations, the ΔV cost from those cases might then be comparable. Or, it may be that the minimum altitude is the crucial factor for a certain range of eccentricities, or that orbital energy should be equal in comparable cases. The answers to these questions lie beyond the scope of this paper; nonetheless, it is important to bring this issue forward. Also, despite this difficulty in making direct case-by-case comparisons, the similarity of the trend of the simulated J_2 ΔV values with the trend of the Keplerian values indicates that the relative dependence of performance on altitude is consistent between the two data sets.

REFERENCES

[1] Wertz, James R. 2001. *Mission Geometry: Orbit and Constellation Design and Management*, El Segundo, CA, and Dordrecht, The Netherlands: Microcosm Press and Kluwer Academic Publishers.

[2] Lange, Benjamin, "The Drag Free Satellite," *AIAA Journal*, Vol. 2, No. 9. Sept. 1964, pp. 1590-1606.

[3] Wertz, James R. and Wiley J. Larson, eds. *Space Mission Analysis and Design, 3rd edition.* El Segundo, CA, and Dordrecht, The Netherlands: Microcosm Press and Kluwer Academic Publisher

[4] Vallado, David A. 2001. *Fundamentals of Astrodynamics and Applications, 2nd edition.* El Segundo, CA, and Dordrecht, The Netherlands: Microcosm Press and Kluwer Academic Publishers.

[5] Fleck, Melissa E. and Scott R. Starin,. "Evaluation of a Drag-Free Concept for Missions in Low Earth Orbit," *Proceedings from the AIAA Guidance, Navigation, and Control Conference*, 11-14 August 2003.